Butane dihedral angle dynamics in water is dominated by internal friction

Jan O. Daldrop[a], Julian Kappler[a], Florian N. Brünig[a], and Roland R. Netz[a,1]

[a]Department of Physics, Freie Universität Berlin, 14195 Berlin, Germany

Edited by Dmitrii E. Makarov, University of Texas, Austin, TX, and accepted by Editorial Board Member Peter J. Rossky April 4, 2018 (received for review December 22, 2017)

The dihedral dynamics of butane in water is known to be rather insensitive to the water viscosity; possible explanations for this involve inertial effects or Kramers' turnover, the finite memory time of friction, and the presence of so-called internal friction. To disentangle these factors, we introduce a method to directly extract the friction memory function from unconstrained simulations in the presence of an arbitrary free-energy landscape. By analysis of the dihedral friction in butane for varying water viscosity, we demonstrate the existence of an internal friction contribution that does not scale linearly with water viscosity. At normal water viscosity, the internal friction turns out to be eight times larger than the solvent friction and thus completely dominates the effective friction. By comparison with simulations of a constrained butane molecule that has the dihedral as the only degree of freedom, we show that internal friction comes from the six additional degrees of freedom in unconstrained butane that are orthogonal to the dihedral angle reaction coordinate. While the insensitivity of butane's dihedral dynamics to water viscosity is solely due to the presence of internal friction, inertial effects nevertheless crucially influence the resultant transition rates. In contrast, non-Markovian effects due to the finite memory time are present but do not significantly influence the dihedral barrier-crossing rate of butane. These results not only settle the character of dihedral dynamics in small solvated molecular systems such as butane, they also have important implications for the folding of polymers and proteins.

molecular friction | reaction rates | memory effects | dihedral angle | generalized Langevin equation

For the understanding of conformational and biochemical reactions, a low-dimensional stochastic description in suitable reaction coordinates is a powerful approach. In particular, in the context of protein folding, diffusion in a one-dimensional free-energy landscape is a prominent model to come to terms with the high-dimensional phase-space dynamics of proteins (1–3). By projection onto a one-dimensional reaction coordinate, orthogonal degrees of freedom produce effective friction and random force contributions (4, 5). These byproducts of projection cannot be neglected, since friction decisively influences reaction rates (6).

Obviously, the friction that characterizes a protein folding coordinate contains contributions from the surrounding solvent as well as from internal protein degrees of freedom (7), but it is less clear how to separately measure these two contributions (experimentally or in simulations). Typically, the prime object in protein studies concerned with friction effects is the folding time τ_{fold}. In the overdamped limit, when inertia and memory effects are neglected, τ_{fold} scales with the effective friction coefficient γ as $\tau_{\mathrm{fold}} \sim \gamma$ (6). By the addition of viscogenic agents, the solvent viscosity η increases relative to the pure water value; assuming that solvent and internal friction are additive according to $\gamma = \gamma_{\mathrm{sol}} + \gamma_{\mathrm{int}}$ and furthermore that Stokes' law holds for the solvent friction contribution, $\gamma_{\mathrm{sol}} \sim \eta$, while γ_{int} is independent of η, the internal contribution γ_{int} can be obtained by linear extrapolation of $\tau_{\mathrm{fold}} \sim \gamma_{\mathrm{sol}} + \gamma_{\mathrm{int}}$ down to vanishing solvent viscosity $\eta \to 0$ (7). Via this definition, internal friction has been demonstrated for various proteins (7–16). In fact, deviations from a linear dependence $\gamma_{\mathrm{sol}} \sim \eta$ have been experimentally observed for some proteins (9), while for other proteins, no internal friction was detected at all (17). Even in simulations, where—in contrast to experiments—the water friction can be reduced and a modification of the folding free-energy landscape with changing viscosity can be excluded, the extrapolation down to vanishing solvent friction is not trivial (18–22).

The above definition of internal friction hinges on a few critical assumptions which are not necessarily satisfied in real systems. (*i*) Inertia effects lead to deviations from the simple law $\tau_{\mathrm{fold}} \sim \gamma$ and to Kramers turnover, which can be misinterpreted as internal friction (23–25). While the effective mass describing a protein reaction coordinate presumably is small, the balance of effective inertial and friction parameters of reaction coordinates that describe complex reactions is not fully understood. (*ii*) Friction will in general not be constant along a reaction coordinate (15, 18, 26), so the linear additivity assumption $\gamma = \gamma_{\mathrm{sol}} + \gamma_{\mathrm{int}}$ not necessarily holds when averaged over the reaction coordinate. (*iii*) Most serious are memory effects, which influence barrier-crossing dynamics (19, 27–29) and can, depending on the value of the memory time, slow down or even accelerate barrier crossing (30), which starkly invalidates the overdamped Kramers scaling $\tau_{\mathrm{fold}} \sim \gamma$.

Previous theoretical approaches to internal friction based on reaction times suffer from the indirect connection between transition times and friction and necessarily rely on various model assumptions (18–22) (not so different from the experimental

Significance

The interpretation of rates of reactions that take place in a solvent is complicated because of the entanglement of free-energy and history-dependent friction effects. In this context, the dihedral dynamics of butane has played a paradigmatic role since it is simple yet relevant for conformational transitions in polymers and proteins. We directly extract the friction that governs the dihedral dynamics in butane from simulations. We show that ∼89% of the total friction cannot be described as solvent friction and is caused by degrees of freedom that are orthogonal to the dihedral reaction coordinate. This shows that the hydrodynamic estimate of friction severely fails, even in the simplest molecular reaction.

Author contributions: J.O.D., J.K., and R.R.N. designed research; J.O.D., J.K., and F.N.B. performed research; J.O.D. contributed new data-analysis tools; J.O.D. analyzed data; and J.O.D. and R.R.N. wrote the paper.

The authors declare no conflict of interest.

This article is a PNAS Direct Submission. D.E.M. is a guest editor invited by the Editorial Board.

[1]To whom correspondence should be addressed. Email: rnetz@physik.fu-berlin.de.

This article contains supporting information online at www.pnas.org/lookup/suppl/doi:10.1073/pnas.1722327115/-/DCSupplemental.

Published online April 30, 2018.

situation). Direly needed are models which allow to check for the presence of internal friction independently of any theoretical assumptions that relate friction to reaction times, as well as methods to extract friction and memory functions directly from simulations instead of inferring friction effects indirectly from measured reaction times.

In this work, we introduce methods to meet both challenges. We consider butane, since it is the simplest molecule that shows a nontrivial conformational transition in a solvent and since it has been a testing ground for theoretical and experimental developments (31–42). In fact, dihedral isomerization rates are quite insensitive to the solvent viscosity (19–22, 24, 43–46), which was first theoretically demonstrated for butane by comparing the reactive fluxes in liquid and frozen organic solvents (36). The origin of this insensitivity was discussed intensely, and it was argued that both inertial and memory effects are relevant (19, 47, 48). We first simulate a single butane molecule in water and compare two scenarios: the free scenario, where all four carbons can freely move, subject to bond length and bond angle constraints, and the constrained scenario, where three carbons are fixed in space and only one terminal carbon can move. While the free-energy landscape for the dihedral is the same in both scenarios, the transition times differ for high water viscosities (which we modify in our simulations by changing the water mass) by a factor of 10. This unequivocally demonstrates that the additional butane degrees of freedom (which are orthogonal to the dihedral angle) in the free scenario significantly change the effective friction along the reaction coordinate. Secondly, we introduce a generalized method to extract the friction memory kernel that couples to the reaction coordinate (26, 49), in our case the dihedral angle, from unconstrained simulation trajectories. A memory kernel accounts for the fact that friction on the molecular scale is not instantaneous but rather depends on the system's history in a non-Markovian manner. Our calculated memory kernels reveal that indeed the friction substantially differs between the constrained and free butane scenarios. The friction coefficients, which follow by an integral over the memory kernels, are used to predict the transition times of the free and constrained butane scenarios in quantitative agreement with direct simulation results; for this, we need to use reaction rate theory that accounts for inertial effects. This shows that our theoretical framework, which simultaneously yields reaction times as well as friction effects, is consistent. Finally, the internal friction contribution is determined by a fit of the extracted total friction versus the water viscosity: For the constrained butane, the internal contribution is negligible, as expected, while for the free butane, the internal contribution overwhelms the solvent contribution by a factor of eight, which explains why the butane dihedral reaction is rather insusceptible to an increase of the water viscosity.

We unambiguously show that the dihedral angle dynamics of a butane molecule is dominated by internal friction, which stems from the coupled dynamics of the four carbons and the solvent. This demonstrates that internal friction exists already for the simplest molecular system that possesses a conformational transition, in line with previous works where dihedral angle isomerization has been argued to be a source of internal friction in protein folding (9, 20–22, 45, 46). In fact, the internal friction contribution for free butane is produced by the rotational and translational butane degrees of freedom, as is further discussed in Conclusions. According to traditional terminology, we call the friction part that does not scale linearly with solvent viscosity the internal friction contribution.

Results and Discussion

Butane Dihedral Barrier-Crossing Times. In our simulations, we place a single butane in a water box. We systematically vary the mass of water molecules m_w while keeping the butane mass fixed. This modifies all intrinsic water time scales and in particular also the water viscosity according to $\eta \propto \sqrt{m_w}$, but leaves all equilibrium distribution functions invariant (18). We use a united-atom force field for butane that neglects the hydrogens and approximates butane by four Lennard–Jones beads that are subject to fixed bond lengths and fixed bond angles; for water, we use the extended simple point charge (SPC/E) model (*Materials and Methods*). We compare the free scenario, where all four butane carbons can move, with the constrained scenario, where three carbons are fixed in space and only one terminal carbon can rotate; see Fig. 1 *A* and *B* for an illustration. The only degree of freedom in the constrained scenario is the dihedral angle, while in the free scenario, one has six additional degrees of freedom, three translational and three orientational. The free-energy profiles in the free and constrained scenarios in Fig. 1*C* perfectly overlap, as expected based on the translational and orientational invariance of the problem, and they reflect the presence of the aqueous solvent (32, 33, 39, 41).

The mean first-passage times τ_{MFP} for the *cis*-to-*trans* transition of the dihedral, as defined in Fig. 1*C* and extracted from the simulation trajectories shown in Fig. 1*D*, are depicted as a function of the rescaled water viscosity η/η_0 in Fig. 2 for the free and constrained scenarios. Here, η_0 denotes the bulk viscosity of water with the normal mass. τ_{MFP} for free butane is rather insensitive to η, in agreement with previous results (19, 36). Constrained butane behaves differently for $\eta > \eta_0$ and shows

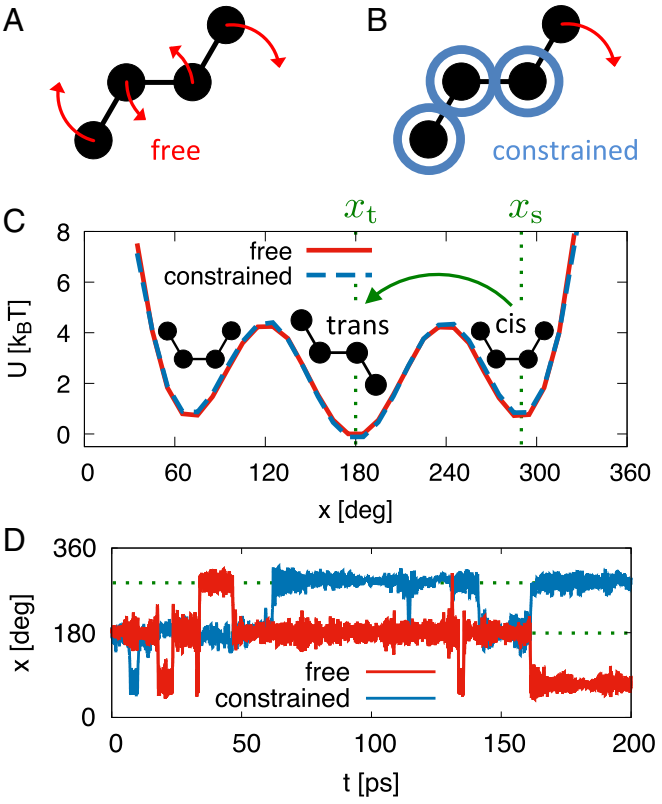

Fig. 1. (*A* and *B*) Schematic illustration of a free butane molecule where all four carbons can move (*A*) and a constrained butane where three carbons are fixed in space and only one terminal carbon can move (*B*). (*C*) Comparison of the free energy *U* as a function of the dihedral angle *x* for the free and constrained butane solvated in SPC/E water, extracted from simulation trajectories. The starting and target angles x_s and x_t for the calculation of the *cis*-to-*trans* dihedral barrier-crossing time are indicated by dotted vertical lines. (*D*) Typical dihedral angle simulation trajectories for free and constrained butane for elevated water viscosity $\eta = \sqrt{10}\eta_0$.

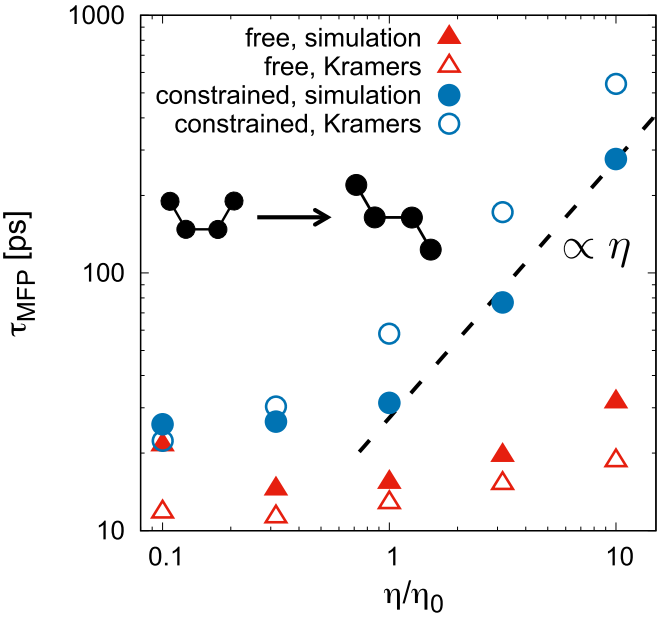

Fig. 2. Mean first passage times τ_{MFP} of the *cis*-to-*trans* transition of the butane dihedral for free (triangles) and constrained (circles) butane extracted from simulation trajectories (filled symbols) are shown as a function of the rescaled water viscosity η/η_0, where η_0 refers to the SPC/E water viscosity. The estimates based on the Kramers formula for medium to strong friction Eq. **5** are included as open symbols.

a linear increase of τ_{MFP} with η (indicated by a broken straight line), while for $\eta < \eta_0$ the results for the free and constrained scenarios are rather similar and depend only weakly on η, which will later be explained by inertial effects (i.e., Kramers turnover). The stark deviation between the free and constrained scenarios for $\eta > \eta_0$, amounting to a difference in the reaction times by a factor of 10 for the highest viscosity $\eta = 10\eta_0$, can only be caused by the six additional degrees of freedom for free butane that are orthogonal to the dihedral angle coordinate. Since the dihedral free energy is the same for both scenarios, we conclude that the friction is different in the two scenarios and that this friction difference is caused by the additional degrees of freedom that are present in the free scenario and absent in the constrained scenario. We will later show that the difference in the total friction between the free and constrained scenarios is accompanied by an internal friction contribution for the free case.

Memory Kernels and Friction Coefficients. To quantify the friction that acts on the dihedral angle, we map the dynamics of the butane dihedral angle x onto the generalized Langevin equation (GLE)

$$m\ddot{x}(t) = -\int_0^t dt'\,\Gamma(t')\dot{x}(t-t') - \nabla U[x(t)] + F_R(t), \qquad [1]$$

where $\Gamma(t)$ denotes the memory kernel. The random force $F_R(t)$ obeys the fluctuation–dissipation theorem and satisfies $\langle F_R(t)F_R(t')\rangle = k_B T\,\Gamma(t-t')$. For vanishing potential, the GLE has been derived by linear projection techniques (4, 5). The mass m is an effective one and follows directly from the simulated dihedral angle trajectory $x(t)$ via the equipartition theorem $m\langle\dot{x}^2\rangle = k_B T$ (*SI Appendix*). The potential $U(x)$ in the GLE is in fact a free energy and follows from the simulated equilibrium probability density along the reaction coordinate, $p(x)$, as $U(x) = -k_B T \log p(x)$ and is shown in Fig. 1*C*. To extract $\Gamma(t)$ from simulation trajectories in the presence of a finite potential $U(x)$, we extend previous methods (26, 49–51). It is crucial that we extract $\Gamma(t)$ without applying constraints along the reaction coordinate x, as the pronounced differences in the barrier-crossing dynamics between free and constrained butane show that constraints decisively influence the system dynamics. In fact, recent simulation work demonstrated that friction is modified by positional constraints even for the simple system of a methane molecule that diffuses in water (52). $\Gamma(t)$ in Eq. **1** does not depend on the reaction coordinate x, which is an approximation that should be rather accurate judged from the weak dependence of calculated memory kernels for butane frozen in different dihedral angle positions (53), in particular compared with the pronounced differences between the kernels for free and constrained butane that will be presented below. To proceed, we multiply Eq. **1** by $\dot{x}(0)$ and average over the noise to obtain

$$m\,\langle\dot{x}(0)\ddot{x}(t)\rangle = -\int_0^t dt'\,\Gamma(t')\,\langle\dot{x}(0)\dot{x}(t-t')\rangle - \langle\dot{x}(0)\nabla U[x(t)]\rangle, \qquad [2]$$

where we used that the random force is not correlated with the initial velocity, i.e., $\langle\dot{x}(0)F_R(t)\rangle = 0$ (4). Discretizing all functions as $\Gamma_i = \Gamma(i\Delta t)$ with a time step Δt we obtain the iteration equation

$$\Gamma_i = -\frac{1}{\omega_{i,i}\Delta t C_0^{\dot{x}\dot{x}}}\left(\sum_{j=0}^{i-1}\omega_{i,j}\Delta t\Gamma_j\,C_{i-j}^{\dot{x}\dot{x}} + mC_i^{\dot{x}\ddot{x}} + C_i^{\dot{x}\nabla U}\right), \qquad [3]$$

where we defined the correlation function $C_i^{\dot{x}\ddot{x}} = \langle\dot{x}(0)\ddot{x}(i\Delta t)\rangle$ (and similarly $C_i^{\dot{x}\dot{x}}$ and $C_i^{\dot{x}\nabla U}$) and the integration weight $w_{i,j} = 1 - \delta_{i,0}/2 - \delta_{i,j}/2$. The correlation function $C_i^{\dot{x}\nabla U} = \langle\dot{x}(0)\nabla U[x(i\Delta t)]\rangle$ is obtained by cubic spline interpolation of $U(x)$. In *SI Appendix*, we demonstrate the numerical robustness of our method.

The extracted memory kernels $\Gamma(t)$ for free butane in Fig. 3*B* are quite similar for different water viscosities, while they differ strongly for constrained butane in Fig. 3*A*. In particular, for free butane, the long time tail of $\Gamma(t)$, which is mostly responsible for the effective friction, is almost independent of η, and oscillations appear that we associate with the presence of orthogonal degrees of freedom. In qualitative accordance with our results in Fig. 2 for the barrier-crossing time, we can say that for free butane, the effective friction is less sensitive to solvent viscosity compared with constrained butane.

In Fig. 4, we show the friction coefficient γ for free and constrained butane as a function of water viscosity, which follows from an integral over the memory function according to $\gamma = \int_0^\infty dt\,\Gamma(t)$. For numerical integration, we fit the long time decay of $\Gamma(t)$ by an exponential function (*SI Appendix*). The friction for constrained butane is linearly proportional to the solvent viscosity, as expected based on simple hydrodynamics: We denote the translational friction coefficient of a methyl group by $\gamma_{trans} = 6\pi\eta R_{CH_3}$. For a methyl group of radius $R_{CH_3} \approx 0.2\,\mathrm{nm}$ that rotates at a fixed bond angle $\alpha = 111°$ and C–C bond length $l_B = 0.15\,\mathrm{nm}$ around a fixed point in space, we estimate the dihedral friction constant $\gamma = (2\pi/360)^2(l_B\sin(\alpha))^2\gamma_{trans} = 0.01\cdot(\eta/\eta_0)\,\mathrm{u\,nm^2/deg^2\,ps}$, not so different from what we extract from the simulations in Fig. 4 for constrained butane. In contrast, the dynamics of free butane is characterized by a friction coefficient that very weakly depends on the water viscosity, in stark contrast to simple hydrodynamics. This failure of hydrodynamics was first inferred from simulations of free butane in an organic solvent (36).

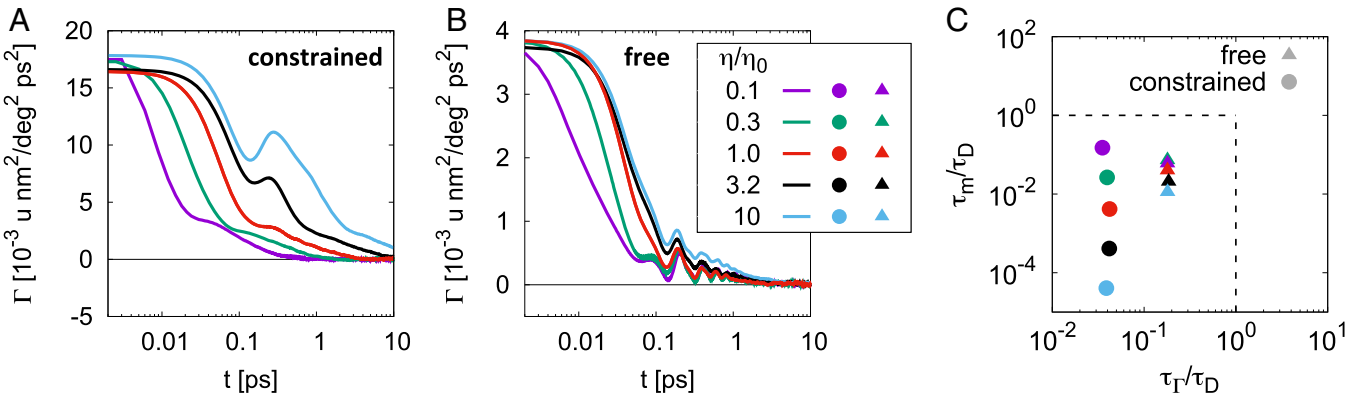

Fig. 3. (*A* and *B*) Memory kernels $\Gamma(t)$ for different rescaled water viscosities η/η_0 extracted from simulation trajectories via Eq. **3** for constrained (*A*) and free (*B*) butane, where η_0 denotes the SPC/E water viscosity. (*C*) Inertial and memory timescale ratios τ_m/τ_D and τ_Γ/τ_D calculated from the memory kernels of free and constrained butane for different viscosities, where τ_D denotes the characteristic diffusion time (same color coding as in *B*).

Internal Versus Solvent Friction. We include empirical fits according to refs. 7, 9, and 12

$$\gamma = (\eta/\eta_0)\gamma_{\mathrm{sol},0} + \gamma_{\mathrm{int}}, \qquad [4]$$

into Fig. 4 as solid lines. The fits are very good, which validates the assumption of additive solvent and internal contributions. For constrained butane, we obtain $\gamma_{\mathrm{int}} = 1.8\cdot10^{-4}\,\mathrm{u\,nm^2/deg^2\,ps}$ and $\gamma_{\mathrm{sol},0} = 3.9\cdot10^{-3}\,\mathrm{u\,nm^2/deg^2\,ps}$, which corresponds to a ratio of $\gamma_{\mathrm{int}}/\gamma_{\mathrm{sol},0} = 0.05$ and shows that internal friction is negligible in this case. A small spurious internal friction contribution is in fact expected even for constrained butane, based on the finite difference between the translational friction coefficient of immobilized and free solutes, as recently demonstrated in simulations of a single methane molecule in water (52). In contrast, for free butane, we find $\gamma_{\mathrm{int}} = 5.2\cdot10^{-4}\,\mathrm{u\,nm^2/deg^2\,ps}$ and $\gamma_{\mathrm{sol},0} = 6.7\cdot10^{-5}\,\mathrm{u\,nm^2/deg^2\,ps}$, and thus a ratio $\gamma_{\mathrm{int}}/\gamma_{\mathrm{sol},0} = 7.7$. Hence, the dynamics of free butane is dominated by internal friction effects for normal water viscosity η_0. The substantial reduction of the solvent friction contribution $\gamma_{\mathrm{sol},0}$ in the free case compared with the constrained case can be rationalized by the fact that the dihedral angle for free butane is a relative coordinate that depends on the motion of all four carbons; it is thus governed by a relative diffusion constant for the constrained molecular motion that results from the weighted sum of the individual carbon atom diffusion constants.

It remains to be checked whether the friction coefficients we extract from simulation trajectories in Fig. 4 explain the dihedral barrier-crossing times in Fig. 2. This is nontrivial in the present case, since, as mentioned earlier, memory and inertia effects invalidate the simple Kramers prediction $\tau_{\mathrm{MFP}} \sim \gamma$. To proceed, it is useful to introduce the characteristic time scales of the system. These are the inertial time $\tau_m = m/\gamma$, that is, the time at which ballistic motion crosses over to diffusive motion; the memory time $\tau_\Gamma = \gamma/\Gamma(0)$, that is, the decay time of the memory kernel; and the diffusive time $\tau_D = L^2\gamma/(k_B T)$, that is, the free-diffusion time to advance over a characteristic angle of $L = 60°$. In Fig. 3*C* we demonstrate that $\tau_m < \tau_D$ and $\tau_\Gamma < \tau_D$ hold for all simulation data, in which case Kramers' formula for the mean first passage time in the medium to strong friction case (6),

$$\tau_{\mathrm{MFP}} = \frac{2\pi\,\omega_{\max}/\omega_{\min}}{[\gamma^2/4m^2 + \omega_{\max}^2]^{1/2} - \gamma/2m}\exp\left(\frac{\Delta U}{k_B T}\right), \qquad [5]$$

is expected to be approximately valid (30), in line with previous theoretical estimates (34–37). For the barrier height, we extract $\Delta U = 3.7\,k_B T$ from the free energy in Fig. 1*C*, $m\omega_{\max}^2 = 6\cdot10^{-3}\,k_B T/\mathrm{deg^2}$ and $m\omega_{\min}^2 = 9\cdot10^{-3}\,k_B T/\mathrm{deg^2}$ are the curvatures of the free energy at the maximum and minimum. The results from Eq. **5** for free and constrained butane are included as open data points in Fig. 2; the comparison with the simulation data is quite good without adjustable parameters. Looking more closely at the comparison, we see that the simulation data in the constrained case show a slightly shorter barrier-crossing time than expected based on the Kramers formula, whereas for free butane we see the opposite. Both trends can be explained based on memory effects (30): For intermediate memory time $\tau_\Gamma/\tau_D \approx 0.001 - 0.1$, as realized for constrained butane (Fig. 3*C*), memory effects significantly accelerate barrier crossing, while a longer memory time $\tau_\Gamma/\tau_D > 0.1$, as realized for free butane (Fig. 3*C*), increases the barrier-crossing time.

The saturation of τ_{MFP} for the constrained case in the low-viscosity limit in Fig. 2 in fact is solely due to inertia effects

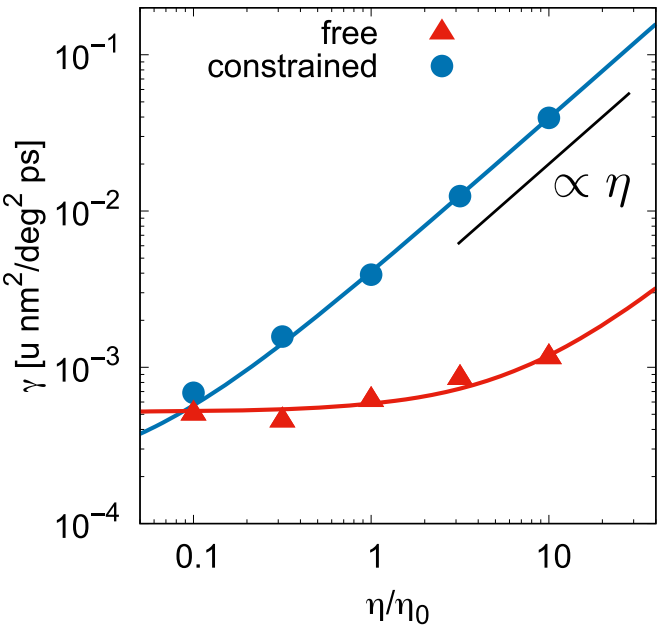

Fig. 4. Friction coefficient γ extracted from the memory kernels in Fig. 3 *A* and *B* as a function of the rescaled water viscosity η/η_0 for free and constrained butane. Empirical fits according to Eq. **4** (denoted by lines) yield internal-to-solvent friction ratios of $\gamma_{\mathrm{int}}/\gamma_{\mathrm{sol},0} = 7.7$ for free and $\gamma_{\mathrm{int}}/\gamma_{\mathrm{sol},0} = 0.05$ for constrained butane.

and thus reflects Kramers turnover. This follows from the fact that the friction γ for the constrained case in Fig. 4 is roughly linear in η over the entire range of water viscosities, so any deviation from the overdamped Kramers prediction $\tau_{\mathrm{MFP}} \sim \eta$ must come from inertia effects. In contrast, the behavior of τ_{MFP} for the free case can only be explained by a combination of inertia and internal friction effects. This shows that the present simulation strategy, which compares the free and constrained scenarios and at the same time extracts memory functions, is necessary and useful.

Conclusions

The dihedral barrier-crossing dynamics of a constrained butane molecule, where only one carbon atom is allowed to move and thus the dihedral angle is the only degree of freedom (besides solvent degrees of freedom), is shown to be very different from the dynamics of a free butane, where a total of seven spatial degrees of freedom are present. This unambiguously demonstrates that friction generated by degrees of freedom that are coupled but orthogonal to the reaction coordinate (in our case, the dihedral angle) is dominant in solvated butane. By monitoring the friction, which we directly extract from the memory kernel, as a function of the solvent viscosity, we show that orthogonal degrees of freedom significantly modify the solvent friction contribution and also produce an additional contribution which does not vanish in the limit of vanishing solvent viscosity. This contribution, defined by the empirical additive formula Eq. **4**, we denote, in analogy to protein folding experiments (7, 9, 12), as internal friction, without implying that this contribution is caused by degrees of freedom that are spatially internal and thereby hidden from the solvent. Rather, the internal friction contribution in butane stems from the dynamic partitioning of energy over all degrees of freedom that are orthogonal to the reaction coordinate, which, in addition to the six spatial (consisting of three translational and three orientational degrees of freedom), also include six conjugate momentum degrees of freedom. In *SI Appendix*, we present simulations where only one carbon atom of butane is fixed and thus translational degrees of freedom are eliminated, while rotations are still possible. These results demonstrate that both translational and orientational degrees of freedom contribute rather equally to the internal friction and at the same time reduce the solvent friction contribution. This is very different from previous studies on the barrier-crossing dynamics of butane in vacuum, since in vacuum, translational degrees of freedom are decoupled because of momentum conservation (40). This means that solvent degrees of freedom strongly couple translational and orientational butane degrees of freedom to the reaction coordinate, in line with previous findings and arguments (36). It is interesting to note that the effect of orthogonal degrees of freedom is rather ambivalent in that it creates internal friction, but at the same time reduces the solvent friction contribution.

Based on our finding that already for the simplest molecule that allows for barrier crossing, internal friction dominates the dynamics, we expect that for larger and more complex molecules, which possess more orthogonal degrees of freedom, internal friction will play an even more important role for the dynamics. For macromolecular conformational transitions, for which the rate-limiting step involves dihedral angle isomerization (20, 24, 25, 54, 55), our findings constitute a mechanism for the emergence of internal friction effects. But other mechanisms, for example, based on interactions between molecular subunits, certainly also exist. Beyond these applications to polymers and proteins, dihedral isomerization of butane is also interesting in its own right and has been studied by 2D infrared spectroscopy (42). The experimental dihedral isomerization time of a butane derivative solvated in CCl_4 was found to be in the $10\,\mathrm{ps}$ range, which agrees with predictions from classical molecular dynamics (MD) simulations (36) and is similar to the simulation results we obtain here. Our analysis thus reveals that in such experiments, the internal friction, which for normal water viscosity makes up $\sim 89\%$ of the total friction, dominates the dynamics, a fact that does not transpire from the simulations per se.

It would be desirable to derive the empirical Eq. **4**, which decomposes the effective friction coefficient that governs a reaction into solvent and internal contributions, from more basic considerations. In the absence of such a derivation, the good comparison between Eq. **4** and the simulation data in Fig. 4 validates the linear additivity thus only in a heuristic sense and could break down for more complicated systems.

Materials and Methods

Simulations are carried out by using the GROMACS (Version 5.1) (56, 57) simulation package with double precision. Butane is parameterized by the GROMOS (58) united atom force field; for water, we use the SPC/E (59). model. All bond angles and bond lengths of water and butane are constrained by using the SHAKE (60) algorithm. The presence of bond angle and bond length vibrations, which we neglect, has been shown to modify the equilibrium dihedral distribution of solvated butane (32) and to also lead to interesting dynamic effects for butane in vacuum (40). Clearly, the proper account of molecular vibrations goes beyond classical simulations; the reason for freezing these internal molecular degrees of freedom in our study is to make the free-energy profiles for constrained and free butane exactly the same. We perform constant number of particles, volume, and temperature (NVT) MD simulations and vary the water molecule mass m_{w} to change the water viscosity. For water mass larger or equal to the normal water mass, we use a time step of 2 fs; for lighter water mass, we lower the time step by a factor $\eta/\eta_0 \propto \sqrt{m_{\mathrm{w}}}$. The typical total trajectory lengths in normal and light water are 40 ns and are elongated in heavy water by a factor that is proportional to η/η_0. The temperature $T = 300\,\mathrm{K}$ is controlled by the velocity rescaling (61) thermostat, which is coupled only to the solvent with a time constant of $\eta/\eta_0 \cdot 1\,\mathrm{ps}$. In *SI Appendix*, we compare results from NVT and constant number of particles, volume, and energy simulations and demonstrate that the ensemble and thus the thermostat have no influence on our results.

ACKNOWLEDGMENTS. This work was supported by Deutsche Forschungsgemeinschaft Grants SFB 1078 and SFB 1114.

1. Bryngelson JD, Wolynes PG (1989) Intermediates and barrier crossing in a random energy model (with applications to protein folding). *J Phys Chem* 93:6902–6915.
2. Bryngelson JD, Onuchic JN, Socci ND, Wolynes PG (1995) Funnels, pathways, and the energy landscape of protein folding: A synthesis. *Proteins* 21:167–195.
3. Dill KA, Chan HS (1997) From Levinthal to pathways to funnels. *Nat Struct Biol* 4:10–19.
4. Mori H (1965) Transport, collective motion, and Brownian motion. *Prog Theor Phys* 33:423–455.
5. Zwanzig R (2001) *Nonequilibrium Statistical Mechanics* (Oxford Univ Press, Oxford).
6. Kramers HA (1940) Brownian motion in a field of force and the diffusion model of chemical reactions. *Physica* 7:284–304.
7. Ansari A, Jones CM, Henry ER, Hofrichter J, Eaton WA (1992) The role of solvent viscosity in the dynamics of protein conformational changes. *Science* 256:1796–1798.
8. Bieri O, et al. (1999) The speed limit for protein folding measured by triplet–triplet energy transfer. *Proc Natl Acad Sci USA* 96:9597–9601.
9. Jas GS, Eaton WA, Hofrichter J (2001) Effect of viscosity on the kinetics of α-helix and β-hairpin formation. *J Phys Chem B* 105:261–272.
10. Pabit SA, Roder H, Hagen SJ (2004) Internal friction controls the speed of protein folding from a compact configuration. *Biochemistry* 43:12532–12538.
11. Qiu L, Hagen SJ (2004) A limiting speed for protein folding at low solvent viscosity. *J Am Chem Soc* 126:3398–3399.
12. Cellmer T, Henry ER, Hofrichter J, Eaton WA (2008) Measuring internal friction of an ultrafast-folding protein. *Proc Natl Acad Sci USA* 105:18320–18325.
13. Wensley BG, et al. (2010) Experimental evidence for a frustrated energy landscape in a three-helix-bundle protein family. *Nature* 463:685–688.
14. Soranno A, et al. (2012) Quantifying internal friction in unfolded and intrinsically disordered proteins with single-molecule spectroscopy. *Proc Natl Acad Sci USA* 109:17800–17806.
15. Borgia A, et al. (2012) Localizing internal friction along the reaction coordinate of protein folding by combining ensemble and single-molecule fluorescence spectroscopy. *Nat Commun* 3:1195.

16. Chung HS, Piana-Agostinetti S, Shaw DE, Eaton WA (2015) Structural origin of slow diffusion in protein folding. *Science* 349:1504–1510.
17. Plaxco KW, Baker D (1998) Limited internal friction in the rate-limiting step of a two-state protein folding reaction. *Proc Natl Acad Sci USA* 95:13591–13596.
18. Schulz JCF, Schmidt L, Best RB, Dzubiella J, Netz RR (2012) Peptide chain dynamics in light and heavy water: Zooming in on internal friction. *J Am Chem Soc* 134:6273–6279.
19. Sancho Dd, Sirur A, Best RB (2014) Molecular origins of internal friction effects on protein-folding rates. *Nat Commun* 5:4307.
20. Echeverria I, Makarov DE, Papoian GA (2014) Concerted dihedral rotations give rise to internal friction in unfolded proteins. *J Am Chem Soc* 136:8708–8713.
21. Zheng W, De Sancho D, Hoppe T, Best RB (2015) Dependence of internal friction on folding mechanism. *J Am Chem Soc* 137:3283–3290.
22. Zheng W, de Sancho D, Best RB (2016) Modulation of folding internal friction by local and global barrier heights. *J Phys Chem Lett* 7:1028–1034.
23. Klimov DK, Thirumalai D (1997) Viscosity dependence of the folding rates of proteins. *Phys Rev Lett* 79:317–320.
24. Portman JJ, Takada S, Wolynes PG (2001) Microscopic theory of protein folding rates. II. Local reaction coordinates and chain dynamics. *J Chem Phys* 114:5082–5096.
25. Best RB, Hummer G (2006) Diffusive model of protein folding dynamics with Kramers turnover in rate. *Phys Rev Lett* 96:228104.
26. Straub JE, Borkovec M, Berne BJ (1987) Calculation of dynamic friction on intramolecular degrees of freedom. *J Phys Chem* 91:4995–4998.
27. Grote RF, Hynes JT (1980) The stable states picture of chemical reactions. II. Rate constants for condensed and gas phase reaction models. *J Chem Phys* 73:2715–2732.
28. Straub JE, Borkovec M, Berne BJ (1986) Non-Markovian activated rate processes: Comparison of current theories with numerical simulation data. *J Chem Phys* 84:1788–1794.
29. Pollak E, Grabert H, Hänggi P (1989) Theory of activated rate processes for arbitrary frequency dependent friction: Solution of the turnover problem. *J Chem Phys* 91:4073–4087.
30. Kappler J, Daldrop JO, Brünig FN, Boehle MD, Netz RR (2018) Memory-induced acceleration and slowdown of barrier crossing. *J Chem Phys* 148:014903.
31. Chandler D (1978) Statistical mechanics of isomerization dynamics in liquids and the transition state approximation. *J Chem Phys* 68:2959–2970.
32. Chandler D, Berne BJ (1979) Comment on the role of constraints on the conformational structure of n-butane in liquid solvents. *J Chem Phys* 71:5386–5387.
33. Rebertus DW, Berne BJ, Chandler D (1979) A molecular dynamics and Monte Carlo study of solvent effects on the conformational equilibrium of n-butane in CCl_4a), b). *J Chem Phys* 70:3395–3400.
34. Montgomery JA, Chandler D, Berne BJ (1979) Trajectory analysis of a kinetic theory for isomerization dynamics in condensed phases. *J Chem Phys* 70:4056–4066.
35. Levy RM, Karplus M, Andrew McCammon J (1979) Diffusive Langevin dynamics of model alkanes. *Chem Phys Lett* 65:4–11.
36. Rosenberg RO, Berne BJ, Chandler D (1980) Isomerization dynamics in liquids by molecular dynamics. *Chem Phys Lett* 75:162–168.
37. Knauss DC, Evans GT (1980) Liquid state torsional dynamics of butane: The Kramers rate and the torsion angle correlation times. *J Chem Phys* 73:3423–3429.
38. Evans GT (1980) Momentum space diffusion equations for chain molecules. *J Chem Phys* 72:3849–3858.
39. Pratt LR, Rosenberg RO, Berne BJ, Chandler D (1980) Comment on the structure of a simple liquid solvent near a n-butane solute molecule. *J Chem Phys* 73:1002–1003.
40. Berne BJ, De Leon N, Rosenberg RO (1982) Isomerization dynamics and the transition to chaos. *J Phys Chem* 86:2166–2177.
41. Rosenberg RO, Mikkilineni R, Berne BJ (1982) Hydrophobic effect on chain folding. The trans to gauche isomerization of n-butane in water. *J Am Chem Soc* 104:7647–7649.
42. Zheng J, Kwak K, Xie J, Fayer MD (2006) Ultrafast carbon-carbon single-bond rotational isomerization in room-temperature solution. *Science* 313:1951–1955.
43. Kuhn W, Kuhn H (1946) Modellmässige deutung der inneren viskosität (der formzähigkeitskonstante) von fadenmolekeln I. *Helv Chim Acta* 29:609–626.
44. Khatri BS, McLeish TCB (2007) Rouse model with internal friction: A coarse grained framework for single biopolymer dynamics. *Macromolecules* 40:6770–6777.
45. Soranno A, et al. (2017) Integrated view of internal friction in unfolded proteins from single-molecule FRET, contact quenching, theory, and simulations. *Proc Natl Acad Sci USA* 114:E1833–E1839.
46. Avdoshenko SM, Das A, Satija R, Papoian GA, Makarov DE (2017) Theoretical and computational validation of the Kuhn barrier friction mechanism in unfolded proteins. *Sci Rep* 7:269.
47. Pastor RW, Karplus M (1989) Inertial effects in butane stochastic dynamics. *J Chem Phys* 91:211–218.
48. Zuckerman DM, Woolf TB (2002) Transition events in butane simulations: Similarities across models. *J Chem Phys* 116:2586–2591.
49. Berne BJ, Harp GD (1970) On the calculation of time correlation functions. *Adv Chem Phys* 17:63–227.
50. Lange OF, Grubmüller H (2006) Collective Langevin dynamics of conformational motions in proteins. *J Chem Phys* 124:214903.
51. Shin HK, Kim C, Talkner P, Lee EK (2010) Brownian motion from molecular dynamics. *Chem Phys* 375:316–326.
52. Daldrop JO, Kowalik BG, Netz RR (2017) External potential modifies friction of molecular solutes in water. *Phys Rev X* 7:041065.
53. Wan SZ, Xu YW, Wang CX, Shi YY (1995) Analysis of friction kernels for n-butane isomerization in water by the generalized Langevin equation. *J Chem Phys* 102:4976–4980.
54. Kuhn W, Kuhn H (1945) Bedeutung beschränkt freier drehbarkeit für die viskosität und strömungsdoppelbrechung von fadenmolekellösungen I. *Helv Chim Acta* 28:1533–1579.
55. Guo Z, Thirumalai D (1995) Kinetics of protein folding: Nucleation mechanism, time scales, and pathways. *Biopolymers* 36:83–102.
56. Hess B, Kutzner C, van der Spoel D, Lindahl E (2008) GROMACS 4: Algorithms for highly efficient, load-balanced, and scalable molecular simulation. *J Chem Theor Comput* 41:435–447.
57. Abraham MJ, et al. (2015) GROMACS: High performance molecular simulations through multi-level parallelism from laptops to supercomputers. *SoftwareX* 1–2:19–25.
58. Oostenbrink C, Villa A, Mark AE, Van Gunsteren WF (2004) A biomolecular force field based on the free enthalpy of hydration and solvation: The GROMOS force-field parameter sets 53A5 and 53A6. *J Comput Chem* 25:1656–1676.
59. Berendsen HJC, Grigera JR, Straatsma TP (1987) The missing term in effective pair potentials. *J Phys Chem* 91:6269–6271.
60. Ryckaert JP, Ciccotti G, Berendsen HJC (1977) Numerical integration of the Cartesian equations of motion of a system with constraints: Molecular dynamics of n-alkanes. *J Comput Phys* 23:327–341.
61. Bussi G, Donadio D, Parrinello M (2007) Canonical sampling through velocity rescaling. *J Chem Phys* 126:014101.